IEEE Photonics Journal
An IEEE Photonics Society Publication

Open Access

A Chirp-Managed Tunable DBR Laser Based on Novel Cascaded Gratings

Volume 10, Number 5, September 2018

Yao Zhu
Congying Feng
Yuze Wu
Yonglin Yu, ***Member, IEEE***

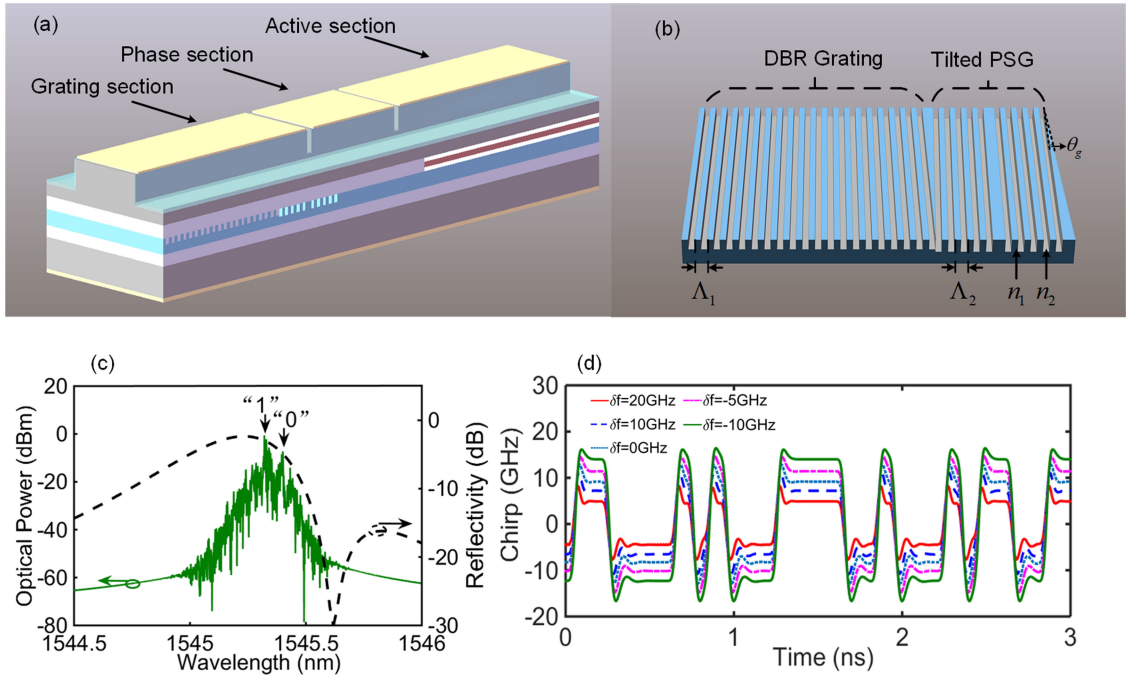

DOI: 10.1109/JPHOT.2018.2871513

A Chirp-Managed Tunable DBR Laser Based on Novel Cascaded Gratings

Yao Zhu, Congying Feng, Yuze Wu, and Yonglin Yu, *Member, IEEE*

Wuhan National Laboratory for Optoelectronics, School of Optical and Electronic Information, Huazhong University of Science and Technology, Wuhan 430074, China

DOI:10.1109/JPHOT.2018.2871513

Manuscript received May 13, 2018; revised June 22, 2018; accepted September 16, 2018. Date of publication September 20, 2018; date of current version October 8, 2018. This work was supported in part by the National Natural Science Foundation of China under Grant 61675073, in part by Fundamental Research Funds for the Central Universities under Grant 2016YXZD004, and in part by the National High Technology Developing Program of China under Grant 2013AA014503. Corresponding author: Yonglin Yu (e-mail: yonglinyu@mail.hust.edu.cn).

Abstract: In this paper, a novel tunable DBR laser based on novel cascaded gratings is proposed for chirp management in high-speed direct modulation applications. The cascaded gratings, i.e., a tilted π phase-shift grating followed by a normal uniform Bragg grating, can provide a narrow-band reflection spectrum with a sharp falling slope on the longer wavelength side, so that the optical spectrum shaping and the detuned-loading effects can be enhanced. Simulation results indicate that the wavelength tuning range of the laser is about 10 nm and the 3-dB modulation bandwidth reaches up to 25 GHz. By simply adjusting the phase current and thus changing the detuned frequency, the extinction ratio and the frequency chirp can be optimized, which is helpful to improve the dispersion tolerance and reduce the dispersion power penalty.

Index Terms: Tunable laser, gratings, direct modulation, chirp management.

1. Introduction

Demands for high capacity transmission are driven by the explosive increase of internet traffic, which has posed great challenge for short-haul local area networks (LANs) and access networks, where multi-Gbps transmission speeds are expected. To meet the increasing demands, 40-Gigabit-capable passive optical networks by 4 $\times$ 10G time and wavelength division multiplexed (TWDM) technology and the 100G Ethernet by 4 $\times$ 25G wavelength division multiplexed (WDM) technology have been proposed by ITU-T G989 Study Group [1] and IEEE 802.3 Working Group [2], respectively, where at least 40 km reach is desired. Directly modulated distributed Bragg reflector (DBR) lasers are expected for short-distance TWDM/WDM system due to their advantages of low manufactory costs, modest wavelength tunability, lower power consumption, less inventory and backup costs and higher output power [3]–[5]. To achieve high capacity transmission, the main issues are focused on boosting the modulation speed of the DBR lasers beyond 10 Gb/s and reducing dispersion power penalty caused by the laser chirp.

Normally the modulation bandwidth of the DBR lasers is limited due to their relative long cavity structure. The detuned-loading effects is an effective way to improve the modulation bandwidth of the DBR lasers, which can be realized by tuning the lasing wavelength on the longer wavelength

side of the reflection spectrum. High speed two-section DBR lasers with a bandwidth of over 30 GHz utilizing the detuned-loading effects have been reported and demonstrated [6], [7]. Another important issue for the directly modulated DBR lasers applied in TWDM/WDM systems is the frequency chirp, which will result in spectrum broaden that severely limits the maximum achievable system transmission capacity due to the fiber dispersion. In our previous work, we proposed a chirp compensated scheme to reduce DBR laser chirp by injecting reverse modulation current into phase section [8]. This method mainly reduces the adiabatic chirp and could extend the transmission distance to 150 km at 2.5 Gb/s, however it would be ineffective when the bitrate is increased up to 10 Gb/s since the transient chirp is dominant at higher modulation speed. Chirp-managed laser (CML) has been demonstrated as a competitive solution to provide high dispersion tolerance for metro/access systems [8], in which a directly modulated laser is followed by an optical spectrum reshaping (OSR) filter. Different directly modulated lasers are used as sources, such as DFB laser [9], tunable modulated-grating Y-branch (MG-Y) lasers [10], DFB laser array [11] and DBR laser [12]. Meanwhile, multi-cavity thin-film filters [13], ring-based filters [14], and optical delay line interferometers [15] are employed as an OSR filter to implement the frequency modulation (FM) to amplitude modulation (AM) conversion to increase the extinction ratio (ER), thereby increasing the dispersion tolerance. Recently, a monolithically integrated CML based on slanted trenches has also been proposed [16].

In this paper, a novel chirp-managed tunable DBR laser is proposed, where a normal DBR section is replaced by a tilted π phase-shift grating cascaded with a normal uniform Bragg grating (named as TPSG-DBR). The reflection spectrum of the TPSG-DBR is significantly narrowed down due to the tilted π phase-shift grating introduced. Static and dynamic characteristics of the proposed tunable TPSG-DBR laser are first simulated and analyzed based on a time-domain traveling-wave model. The wavelength tuning range of the laser is about 10 nm with 8 accessible ITU-channels (100 GHz spacing). The 3-dB modulation bandwidth of the device is above 25 GHz. Compared with the normal DBR design, the TPSG-DBR provides a narrower and asymmetric reflection spectrum. When the operating wavelength of the tunable laser is located on the falling edge of the reflection spectrum, the optical spectrum shaping and the detuned-loading effects can be enhanced to improve ER and suppress the chirp. Finally, reduced dispersion power penalty is demonstrated with the proposed device for different transmission distances over standard single mode fiber (SSMF).

2. Principles and Design of the Cascaded Gratings

As mentioned above, the modulation bandwidth of the DBR lasers can be increased by the so-called detuned loading effects. This is because that the differential gain parameter can be effectively increased under modulation, when the laser is adjusted to work on the long-wavelength side of the reflection peak of the DBR reflector. On the other hand, when the lasing wavelength is located on the falling edge of the reflection spectrum, the falling edge of the reflection spectrum can have filtering effect on the broaden spectrum caused by the laser chirp under modulation. In other words, the DBR reflector can also act as an intra-cavity OSR filter. However, this effect is not obvious in the normal DBR lasers, since the reflection spectrum of the normal DBR reflector with uniform grating do not have a steep slope as required by the OSR filter. To enhance the OSR effect, we propose a novel tunable DBR laser, i.e., TPSG-DBR tunable laser, as illustrated in Fig. 1, where the normal uniform DBR grating is replaced by cascaded gratings consisting of a tilted π phase-shift Bragg grating (PSG) and a normal uniform Bragg grating.

The transmission spectrum of PSG has a very narrow passband in the central wavelength, this characteristic makes PSG a good choice for narrow band filters with sharp falling slope [17]. When the PSG is fabricated within the laser cavity, the residual reflection of PSG is not expected since it will cause serious oscillation of output power. Gratings with a tilted angle can help to reduce the reflection [18], [19], so we introduce a small tilted angle into the PSG. The tilted angle of waveguide gratings is an important factor in determining the grating coupling coefficient [20]. For reflective mode, a small tilted angle will dramatically increase the coupling from fundamental mode to higher order mode, while in single-mode waveguide, higher order modes will quickly fade, the

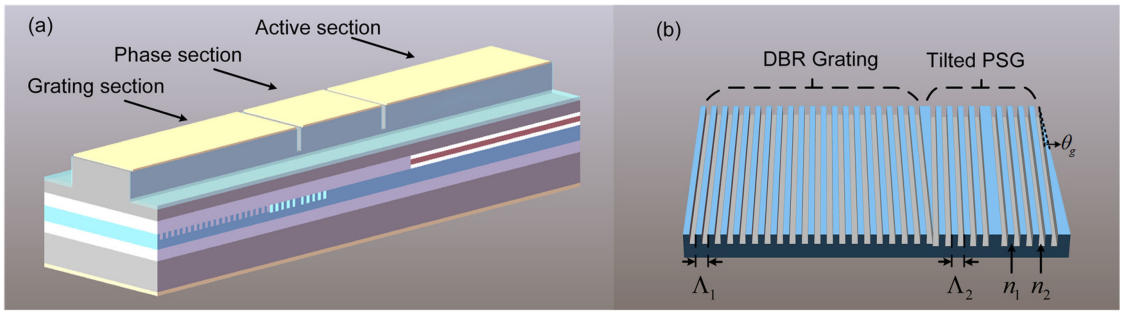

Fig. 1. (a) Schematic diagram of the proposed tunable laser. (b) Structure of the cascaded gratings: TPSG-DBR.

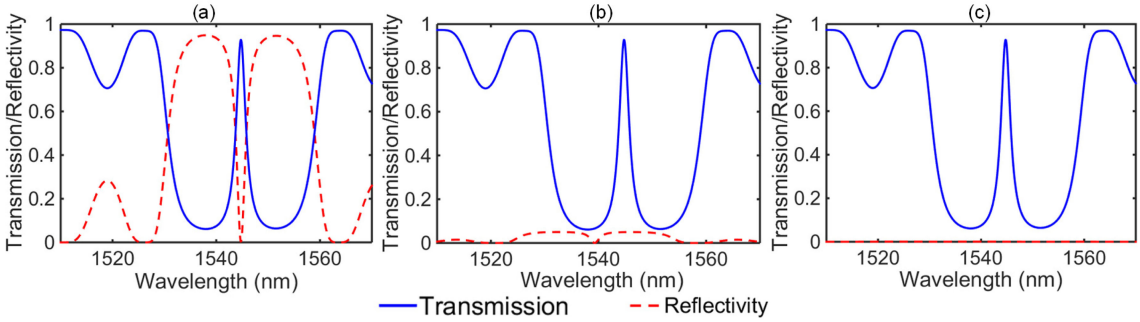

Fig. 2. Transmission and reflection spectrum of the tilted PSG with different tilted angles. (a) $\theta_g = 0^\circ$. (b) $\theta_g = 2^\circ$. (c) $\theta_g = 4^\circ$.

reflectivity will drop rapidly. For transmission mode, the tilted angle should be much larger for strong coupling from fundamental mode to higher order mode, so a small tilted angle of the gratings can have small influences on the transmission mode. Fig. 2 shows the transmission and reflection spectrum of the tilted PSG with different tilted angle θ_g ranging from 0° to 4°, which is calculated by using transmission matrix model (TMM) with tilted incident light [21]. Clearly from Fig. 2, we can observe that the reflectivity drops rapidly as the tilted angle increases. When $\theta_g = 4^\circ$, the reflectivity will become less than -35 dB, while the transmittance changes little. Simulated results indicate that a tilted angle of 4° is enough to remove most of the reflection power out of the laser cavity, so this tilted angle is adopted for laser design.

The total reflectivity coefficient r_{total} of the TPSG-DBR can be calculated by:

$$r_{total} = t_{PSG} \cdot r_{DBR} \cdot t_{PSG}. \tag{1}$$

where t_{PSG} represents the transmission coefficient of the tilted PSG, r_{DBR} represents the reflection coefficient of the uniform Bragg grating. The total reflection spectrum of the TPSG-DBR is presented in Fig. 3, the related parameters are listed in Table 1. The center wavelength of the tilted PSG is designed near the falling edge of the reflection spectrum of the DBR grating to get a steep falling edge. Compared with the normal DBR grating, the reflection spectrum of the TPSG-DBR is significantly narrowed down with a FWHM of about 0.4 nm and the slope of the falling edge is about 0.35 dB/GHz at the -3 dB point.

3. Numerical Simulation of the Tunable TPSG-DBR Laser

3.1 Simulation Model

As shown in Fig. 4, the active and phase section is modeled by a large signal time-domain travelling-wave (TDTW) model, and the cascaded gratings are first simulated by TMM and then transform

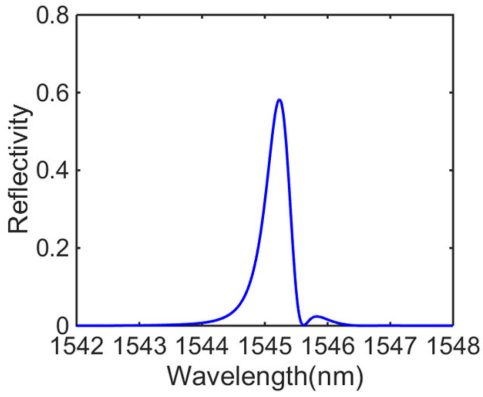

Fig. 3. Reflection spectrum of TPSG-DBR.

TABLE 1
Parameters of the Tunable TSPG-DBR Laser Used in the Simulation

Parameter	Sym bol	Value
Length of the active section	L_a	300 μ m
Length of the phase layer	L_p	60 μm
Thickness of the active layer	d_a	48 nm
Width of the active layer	W_a	1.2 μm
Length of the tilted PSG	L_t	40 μm
Length of the DBR grating	L_{DBR}	300 μm
Period of the DBR grating	Λ_1	235 nm
Period of the tilted PSG	Λ_2	240 nm
Effective refraction index	n_1	3.2723
Effective refraction index	n_2	3.2242
Monomolecul ar recombination coefficient	A	1×10^{8} s-1
Bimolecul ar recombination coefficient	B	8×10^{-17} m^3s^{-1}
Auger recombination coefficient	C	7.5×10^{-41} m^6s^{-1}
Index derivat ive with respect to carrier density	dn/dN	-1.5×10^{-26} m^3
Gain coefficient	g_0	2000 cm^{-1}
Absorption and scattering loss in active layer	α	20 cm^{-1}
Absorption and scattering loss in passive layer	α_p	3 cm^{-1}
Waveguide confinement factor in active layer	Γ_a	0.12
Waveguide confinement factor in passive section	Γ_p	0.3
Transparency carrier density	N_{tr}	1.8×10^{-24} m^{-3}
Effective refractive index	n_{eff0}	3.283
Group refractive index	n_g	3.7
Linewidth enhancement factor	α_H	4
Nonlinear gain saturation coefficient	ε	8×10^{-23} m^3
Reference wavelength	λ_0	1544 nm
Reflection coefficient of the cleavage plane	r_L	0.565

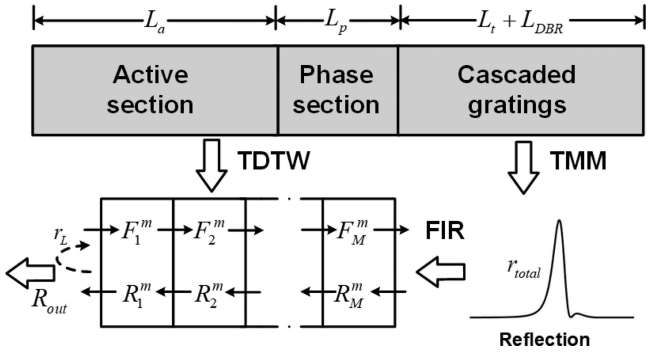

Fig. 4. Schematic diagram of the laser model.

into time domain via the finite impulse response (FIR) digital filter approach [22]. The time-domain travelling wave formula is as follows [23], [24]:

$$\frac{1}{v_g}\frac{\partial F(z,t)}{\partial t}+\frac{\partial F(z,t)}{\partial z}=(\Gamma_a g-\alpha-j\delta)F(z,t)+S_F(z,t). \tag{2}$$

$$\frac{1}{v_g}\frac{\partial R(z,t)}{\partial t}-\frac{\partial R(z,t)}{\partial z}=(\Gamma_a g-\alpha-j\delta)R(z,t)+S_R(z,t). \tag{3}$$

where v_g is the group velocity, F and R represent the forward and backward propagating field inside the waveguide, respectively. S_F and S_R are the spontaneous emission noise coupled into the forward and reverse fields. Γ is the optical field confinement, α is the internal loss, g is the optical field gain (for phase section the gain is zero) and δ is the detuning factor given by:

$$g(z,t)=\frac{g_0\ln\left(N(z,t)/N_{tr}\right)}{2(1+\varepsilon S)}. \tag{4}$$

$$\delta=\frac{2\pi}{\lambda_0}\left(n_{eff}(z,t)-n_{eff\,0}\right). \tag{5}$$

where g_0 is the gain coefficient, c is the speed of light in vacuum, P is the photon density given by the normalized power $\{|F|^2+|R|^2\}$, λ_0 is the reference wavelength, $n_{eff\,0}$ is the initial effective refractive index at transparency. n_{eff} is the effective refractive index related to the carrier density by:

$$\text{Active section}: \quad n_{eff\,(a)}(z,t)=n_{eff\,0}-\frac{\lambda_0}{4\pi}\Gamma_a\alpha_H g_0\ln\left(N(z,t)/N_{tr}\right). \tag{6}$$

$$\text{Phase section}: \quad n_{eff\,(p)}(z,t)=n_{eff\,0}+\Gamma_p\,dn/dN\,N_p. \tag{7}$$

where α_H represents the linewidth enhancement factor, dn/dN is the refractive index derivative with respect to the carrier density and N_p is the carrier density of the phase section.

The time-dependent carrier rate equations in the active layer is described as follows:

$$\frac{dN(t)}{dt}=\frac{I}{eV_a}-AN-BN^2-CN^3-\frac{v_g g_0\ln\left(N(z,t)/N_{tr}\right)P}{1+\varepsilon P}. \tag{8}$$

where I is the injection current of the active section, V_a is the volume of the active layer, A is the monomolecular recombination coefficient, B is the bimolecular recombination coefficient and C is the auger recombination coefficient.

The reflection optical field R^m at specific time m can be expressed by convolution of the incident light field F^k with reflection coefficient in time domain as:

$$R^m=\sum_{k=0}^{M_t} r^k F^{m-k}. \tag{9}$$

where M_t is the length of the coefficient, r is the filter coefficient in time domain, which is the inverse Fourier transform of the reflection coefficient in frequency domain as:

$$r(k) = \frac{1}{M_t} \sum_{k=0}^{M_t} r_{total}(f)\, e^{j2\pi kf\Delta t}. \tag{10}$$

The boundary conditions then become:

$$F(0, t) = r_L R(0, t). \tag{11}$$

$$R(L, t) = \sum_{k=0}^{M_t} r^k F^{t-k}. \tag{12}$$

where r_L is the facet reflectivity at the output end-face, $L = L_a + L_p$ is the length of the active section and phase section.

The detailed parameters used in the simulation are listed in Table 1. The output end-face of the laser is the cleavage plane and the end-face of the grating section is anti-reflection coated with zero reflection. By substituting equations (9)–(12) to the equations (2), (3) and (8), the optical field F and R can be solved, and the static characteristics, including lasing wavelength and optical spectrum, can be obtained by fast Fourier transform of the optical field.

Furthermore, the small signal intensity modulation responses of the tunable laser can be obtained by applying a small sinusoidal perturbation in the TDTW model. Meanwhile, the frequency chirp $\Delta\nu(t)$ of the proposed laser under direct modulation can be expressed as:

$$\Delta\nu(t) = \frac{\alpha_{eff}}{4\pi} \left\{ \frac{1}{P_{out}(t)} \frac{dP_{out}(t)}{dt} + \kappa_c P_{out}(t) \right\}. \tag{13}$$

where P_{out} is the output power, $\kappa_c = 2\Gamma_a \varepsilon / \eta_d h\nu V_a$ is the adiabatic chirp coefficient, η_d is the differential quantum efficiency and ν is the lasing frequency. It should be note that the effective linewidth enhancement factor α_{eff} is related to the slope of the reflection spectrum, which is expressed as [25]:

$$\alpha_{eff} = \frac{\mathrm{Im}\left\{(1 + j\alpha_H)/\chi\right\}}{\mathrm{Re}\left\{(1 + j\alpha_H)/\chi\right\}}. \tag{14}$$

where $\chi = 1 + \frac{\partial}{\partial\omega} ln(r_{total}) / \frac{\partial}{\partial\omega} ln(r_e)$, r_e is the equivalent reflectivity of the active section and phase section given by $r_e = r_L\, e^{-2j(k_1 L_a + k_2 L_p)}$. k_1 and k_2 are the complex wavenumber for the active section and phase section given by $k_1 = \frac{\omega}{c} n_{eff(a)} + j\frac{1}{2}(g - \alpha)$ and $k_2 = \frac{\omega}{c} n_{eff(p)} - j\frac{1}{2}\alpha_p$, respectively.

As shown in Fig. 1 and Table 1, the proposed laser is designed with ridge waveguide structure, and a narrow ridge waveguide (1.2 μm) is initially selected, mainly considering requirements of the single transverse mode condition and high-speed modulation. However, a wider waveguide design (about 2−2.4 μm) will be feasible since operation with the single transverse mode finally determined by gain/loss ratios of the laser. The optical field confinement factor and the effective refraction index slightly increase with increasing the ridge width, which will result in slight changes in parameters of the proposed gratings. So there will be an optimization between the waveguide design and the grating design. In terms of fabrication process, the TPSG-DBR laser has no special requirements compared to a normal DBR laser. However, due to the introduction of the tilted grating, it will require a further step overlay alignment during the fabrication process of the passive grating region.

3.2 Static Characteristics

The wavelength tuning curves with different injection current applied to the grating section and the phase section are shown in Fig. 5(a) and Fig. 5(b), respectively, where the injection current of the active section is 50 mA. Obviously, the longitudinal mode space is about 50 GHz and the total wavelength tuning range is about 10 nm. An example of the superimposed lasing spectrum of 8 ITU channels with channel spacing of 100 GHz is presented in Fig. 6.

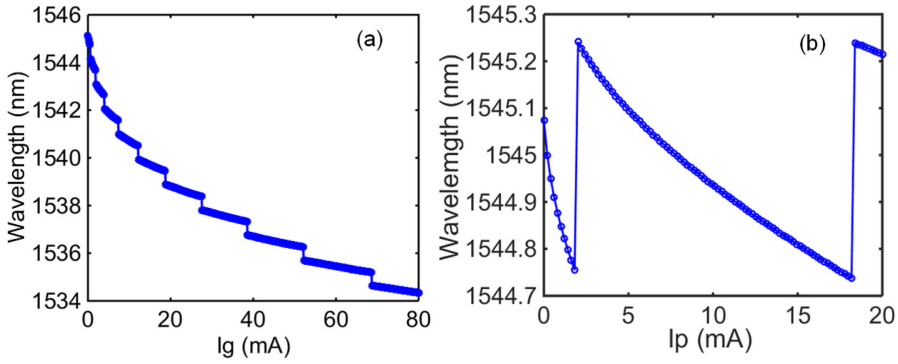

Fig. 5. Wavelength tuning with (a) grating section current Ig and (b) phase section current Ip.

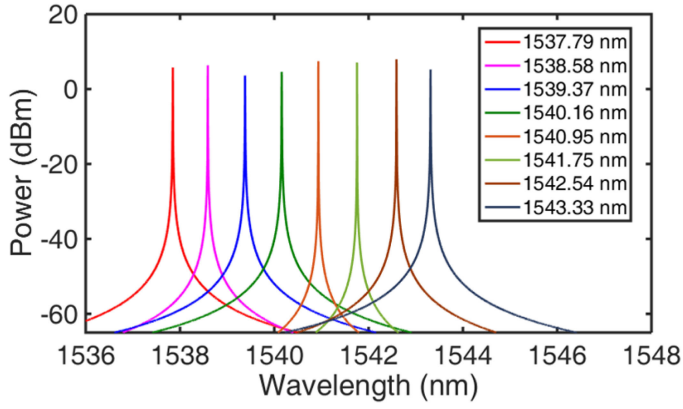

Fig. 6. Superimposed lasing spectrum of 8 ITU wavelength channels (100 GHz spacing).

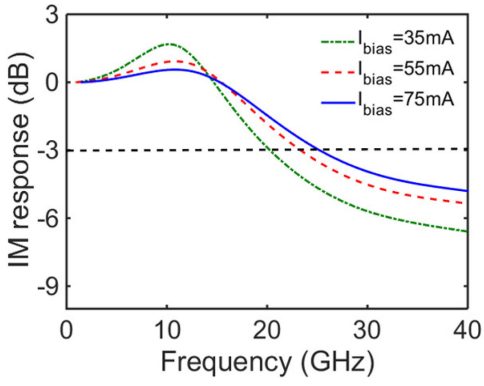

Fig. 7. Small signal intensity modulation response of the laser.

3.3 Modulation Response and Eye-Diagram

To calculate the small signal intensity modulation responses of the tunable TPSG-DBR laser, a small sinusoidal perturbation current is coupled to the bias current of the active section. Fig. 7 shows the response curves under different bias currents, where the currents injected into the phase section and the grating section are 20 mA and 10 mA to ensure the lasing wavelength located at the falling edge of the total reflection spectrum. The 3-dB modulation bandwidth is found to be more than 25 GHz with the bias current I_{bias} up to 75 mA because of the detuned-loading effects. Fig. 8

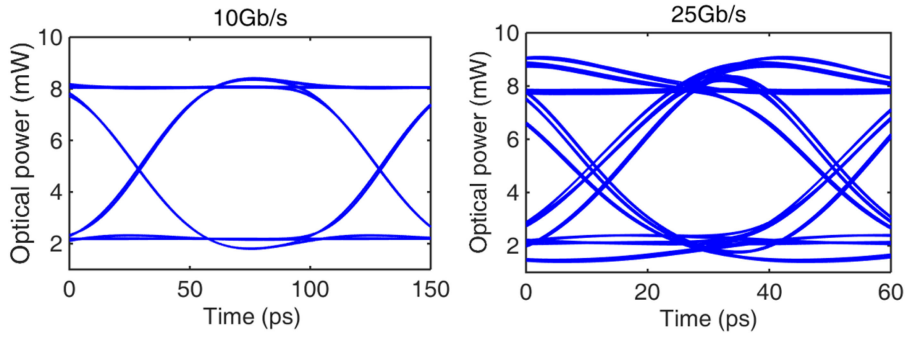

Fig. 8. Eye diagrams of the laser modulated at 10 Gb/s and 25 Gb/s.

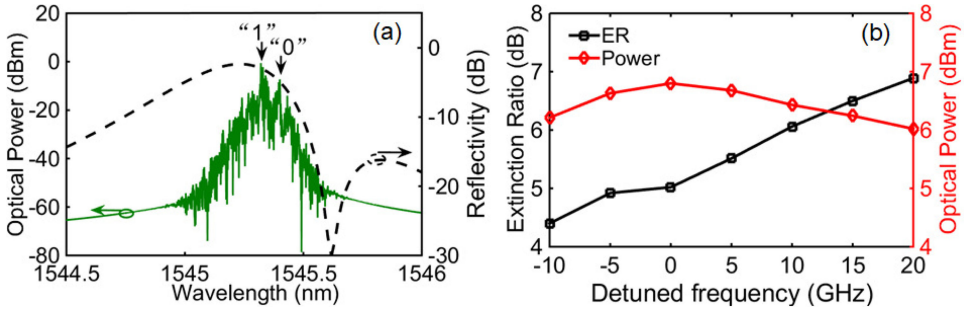

Fig. 9. (a) Reflection spectrum of the TPSG-DBR and optical spectrum of the laser modulated at 10 Gb/s. (b) The output power and the extinction ratio of the laser with different detuned frequencies.

presents the eye diagrams of the laser modulated at 10 Gb/s and 25 Gb/s, where the bias current is set to be 55 mA and the modulation amplitude is 50 mA, the currents into the phase section and grating section are still 20 mA and 10 mA, respectively. Clearly, the eyes of the 10 Gb/s and 25 Gb/s are all well opened.

3.4 Improvements on ER, Chirp and Transmission Performances

The optical spectrum of the laser output modulated at 10 Gb/s superposed with the total reflection spectrum of the TPSG-DBR is presented in Fig. 9(a). It is obvious that due to the laser chirp, the lasing wavelength corresponding to bit "1" is a little shorter than that corresponding to bit "0" during direct modulation. The TPSG-DBR is so designed that the grating reflectivity at bit "1" is much higher than bit "0" to enhance the OSR effect. The output power and the ER of the laser with different detuned frequencies is then studied and the results are presented in Fig. 9(b), where the detuning frequency δf refers to the frequency difference between the center of lasing wavelength and the peak of the reflection spectrum and the positive detuning represents red shift. Distinguished from the normal CMLs, the detuning frequency of the proposed device can be adjusted by simply tuning the phase section current. It suggests that a red shift frequency detuning can help to increase the ER of the laser while a blue shift frequency detuning is just the opposite. However, the frequency detuning can also slightly reduce the output power due to the decrease of the reflectivity. The ER can be optimized by selecting the detuned frequency δf via adjusting the tuning current of the phase section, for example, the ER for the case of Fig. 8 is about 6.2 dB when δf is selected as 12 GHz.

Another interesting phenomenon, i.e., frequency chirp reduction is also observed from Fig. 10, where the effective linewidth enhancement factor and the frequency chirp of the TPSG-DBR laser with different detuned frequencies are calculated based on Eq. (13)–(14). It is obvious from Fig. 10(b) that the frequency chirp, including the transient chirp and the adiabatic chirp can be significantly reduced when a large red shift frequency detuning is selected. This can be understood from the

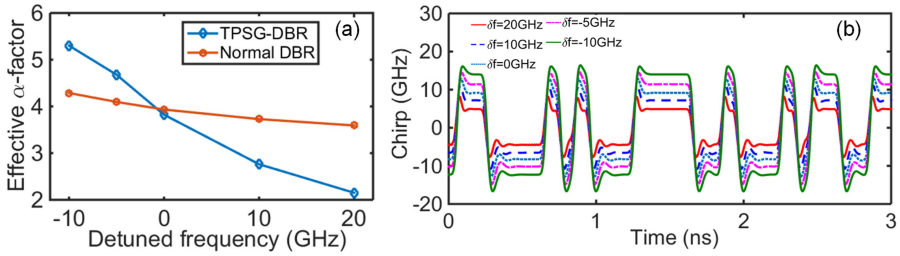

Fig. 10. (a) Effective linewidth enhancement factor. (b) Laser chirp with different detuned frequencies.

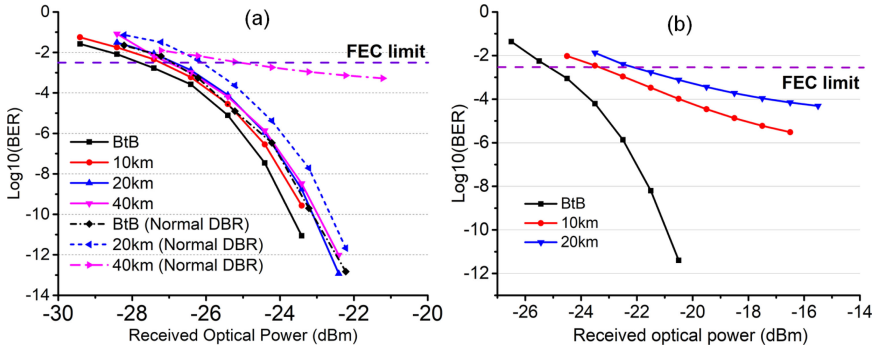

Fig. 11. Calculated BER of different transmission distance with the TPSG-DBR laser modulated at (a) 10 Gb/s, (b) 25 Gb/s.

comparison of the effective linewidth enhancement factor of the TPSG-DBR laser and normal DBR laser in Fig. 10(a). In the range of red shift frequency detuning, the effective linewidth enhancement factor of the TPSG-DBR laser is smaller than that of the normal DBR laser, thus reducing the frequency chirp.

Obviously, compared with the normal DBR design, the TPSG-DBR provide a narrower and asymmetric reflection spectrum. When the operating wavelength of the tunable laser is located on the sharp falling edge of the reflection spectrum, the optical spectrum reshaping can be enhanced to improve ER, at the same time, the laser chirp can be suppressed due to the detuned loading effects. It should be noted that different waveguide design will induce slight differences on modulation performances, such as the speed and the chirp, since related factors (including the relaxation oscillation frequency, the photon lifetime and the optical field confinement factor) will change with the waveguide design.

Transmission simulations are then performed with δf of 12 GHz, making sure that the ER is higher than 6.2 dB. The simulated transmission performances of the proposed laser modulated at 10 Gb/s and 25 Gb/s through SSMF with different transmission distances are shown in Fig. 11(a) and (b), respectively. When the laser is modulated at 10 Gb/s, it is observed that the dispersion power penalty at the receiver is less than 1 dB at the 7% forward error correction (FEC) limit (BER at 3.8×10^{-3}) with the transmission distance increasing from 0 to 40 km. Furthermore, transmission performances of a normal DBR laser with similar structure parameters modulated at 10 Gb/s are added in Fig. 11(a). Clearly, the power penalty for the normal DBR laser with 40 km is larger than 2 dB. When the laser is modulated at 25 Gb/s, the dispersion power penalty is increased to about 2 dB at the FEC limit for 10 km.

4. Conclusions

We have proposed a tunable laser with a grating section consisting of a tilted PSG and a uniform Bragg grating. By slightly tilting the PSG with a tilt angle of 4°, a narrow band reflection spectrum with sharp slope on the longer wavelength side of the total reflectivity peak can be obtained.

When the operating wavelength of the tunable laser is located on the falling edge of the reflection spectrum, i.e., utilizing the detuned-loading effects, the direct modulation bandwidth of the laser reaches up to 25 GHz. More importantly, the optical spectrum shaping and the detuned-loading effects can be enhanced by the TPSG-DBR design. By simply adjusting the phase current and thus changing the detuned frequency, the extinction ratio and the frequency chirp can be optimized. The transmission results have shown that the proposed laser can send 10 Gb/s signal over 40 km SSMF with dispersion power penalty of less than 1 dB, and 25 Gb/s signal over 10 km SSMF with dispersion power penalty of about 2 dB. Thus, the proposed tunable laser is promising for the future short-haul transmission and access network applications, such as TWDM-PON and 100G EPON systems.

References

[1] D. Nesset, "NG-PON2 technology and standard," *IEEE J. Lightw. Technol.*, vol. 33, no. 5, pp. 1136–1143, Mar. 2015.
[2] C. Knittle, "IEEE 100 Gb/s EPON," in *Proc. Opt. Fiber Commun. Conf.*, 2016, pp. 1–6.
[3] Y. Matsui *et al.*, "Transceiver for NG-PON2: Wavelength tunablity for burst mode TWDM and point-to-point WDM," in *Proc. Opt. Fiber Commun. Conf.*, 2016, pp. 1–3.
[4] N. Cheng *et al.*, "Flexible TWDM PON with load balancing and power saving," in *Proc. 39th Eur. Conf. Exhib. Opt. Commun.*, 2013, pp. 1–3.
[5] N. Cheng, X. Yan, N. Chand, and F. Effenberger, "10 Gb/s upstream transmission in TWDM PON using duobinary and PAM-4 modulations with directly modulated tunable DBR laser," in *Proc. Asia Commun. Photon. Conf.*, 2013, Paper ATh3E-4.
[6] O. Kjebon, R. Schatz, S. Lourdudoss, S. Nilsson, B. Stalnacke, and L. Backbom, "30 GHz direct modulation bandwidth in detuned loaded InGaAsP DBR lasers at 1.55 μm wavelength," *IEEE Electron. Lett.*, vol. 33, no. 6, pp. 488–489, Mar. 1997.
[7] U. Feiste, "Optimization of modulation bandwidth in DBR lasers with detuned Bragg reflectors," *IEEE J. Quantum Electron.*, vol. 34, no. 12, pp. 2371–2379, Dec. 1998.
[8] H. Zhao, S. Hu, J. Zhao, Y. Zhu, Y. Yu, and L. P. Barry, "Chirp-compensated DBR lasers for TWDM-PON applications," *IEEE Photon. J.*, vol. 7, no. 1, Feb. 2015, Art. no. 7900809.
[9] Y. Matsui *et al.*, "Chirp-managed directly modulated laser (CML)," *IEEE Photon. Technol. Lett.*, vol. 18, no. 2, pp. 385–387, Jan. 2006.
[10] Y. Matsui *et al.*, "Widely tuneable modulated grating Y-branch chirp managed laser," in *Proc. 35th Eur. Conf. Opt. Commun.*, 2009, pp. 1–2.
[11] D. Mahgerefteh *et al.*, "Tunable chirp managed laser," *IEEE Photon. Technol. Lett.*, vol. 20, no. 2, pp. 108–110, Jan. 2008.
[12] W. Jia, Y. Matsui, D. Mahgerefteh, I. Lyubomirsky, and C. Chan, "Generation and transmission of 10-gbaud optical 3/4-RZ-DQPSK signals using a chirp-managed DBR laser," *IEEE J. Lightw. Technol.*, vol. 30, no. 21, pp. 3299–3305, Nov. 2012.
[13] D. Mahgerefteh *et al.*, "Error-free 250 km transmission in standard fibre using compact 10 Gbit/s chirp-managed directly modulated lasers (CML) at 1550 nm," *Electron. Lett.*, vol. 41, no. 9, pp. 543–544, 2005.
[14] Y. Yokoyama *et al.*, "10.709-Gb/s-300-km transmission of PLC-based chirp-managed laser packaged in pluggable transceiver without any optical or electrical dispersion compensation," in *Proc. 34th Eur. Conf. Exhib. Opt. Commun.*, 2008, pp. 1–2.
[15] X. Zheng *et al.*, "Generation of RZ-AMI using a widely tuneable modulated grating Y-branch chirp managed laser," in *Proc. Opt. Fiber Commun. Conf.*, 2010, Paper OThE5.
[16] Y. Pan, Y. Xi, and X. Li, "Monolithically integrated chirp-managed laser based on a resonant tunneling filter," *Opt. Rev.*, vol. 24, no. 4, pp. 549–553, 2017.
[17] X. Wang, W. Shi, S. Grist, H. Yun, N. A. F. Jaeger, and L. Chrostowski, "Narrow-band transmission filter using phase-shifted Bragg gratings in SOI waveguide," in *Proc. IEEE Photon. Conf.*, Oct. 2011, pp. 869–870.
[18] C. W. Haggans, H. Singh, W. F. Varner, Y. Li, and M. Zippin, "Narrow-band rejection filters with negligible backreflection using tilted photoinduced gratings in single-mode fibers," *IEEE Photon. Technol. Lett.*, vol. 10, no. 5, pp. 690–692, May 1998.
[19] Y. Pan, Y. Xi, and X. Li, "Detuned grating single-mode laser with high immunity to external optical feedback," *IEEE Photon. J.*, vol. 7, no. 6, Dec. 2015, Art. no. 1504013.
[20] K. S. Lee, "Mode coupling in tilted planar waveguide gratings," *Appl. Opt.*, vol. 39, no. 33, pp. 6144–6149, 2000.
[21] P. Yeh, *Optical Waves in Layered Media*. Hoboken, NJ, USA: Wiley, 1988, ch. 6.
[22] W. Li, W. Huang, and X. Li, "Digital filter approach for Simulation of a complex integrated laser diode based on the traveling-wave model," *IEEE J. Quantum Electron.*, vol. 40, no. 5, pp. 473–480, May 2004.
[23] J. Zhao, K. Shi, Y. Yu, and L. P. Barry, "Theoretical analysis of tunable three-section slotted fabry perot lasers based on time-domain traveling-wave model," *IEEE J. Sel. Topics Quantum Electron.*, vol. 19, no. 5, pp. 1–8, Sep./Oct. 2013.
[24] L. M. Zhang, S. F. Yu, M. C. Nowell, D. D. Marcenac, J. E. Carroll, and R. G. S. Plumb, "Dynamic analysis of radiation and side-mode suppression in a second-order DFB laser using time-domain large-signal traveling wave model," *IEEE J. Quantum Electron.*, vol. 30, no. 6, pp. 1389–1395, Jun. 1994.
[25] J. Verdiell, U. Koren, and T. Koch, "Linewidth and alpha-factor of detuned-loaded DBR lasers," *IEEE Photon. Technol. Lett.*, vol. 4, no. 4, pp. 302–305, Apr. 1992.